

Bound-to-bound and bound-to-free transitions in surface photovoltage spectra: Determination of the band offsets for $\text{In}_x\text{Ga}_{1-x}\text{As}$ and $\text{In}_x\text{Ga}_{1-x}\text{As}_{1-y}\text{N}_y$ quantum wells

Massimo Galluppi,* Lutz Geelhaar, and Henning Riechert
Infineon Technologies, Corporate Research, 81730 Munich, Germany

Michael Hetterich and Andreas Grau
*Institut für Angewandte Physik and Center for Functional Nanostructures (CFN), Universität Karlsruhe (TH),
 76131 Karlsruhe, Germany*

Stefan Birner
Walter Schottky Institute and Physics Department, Technical University of Munich, Am Coulombwall 3, 85748 Garching, Germany

Wolfgang Stolz
Department of Physics and Material Science, Philipps-University Marburg, 35032 Marburg, Germany
 (Received 20 June 2005; revised manuscript received 1 September 2005; published 25 October 2005)

We present an extensive study leading to a general understanding about the optical transitions involved in the surface photovoltage (SPV) spectra of type-I quantum well (QW) structures. SPV measurements were carried out on $\text{In}_{0.3}\text{Ga}_{0.7}\text{As}/\text{GaAs}$ QW samples with varying QW width and on $\text{In}_{0.15}\text{GaAs}_{0.85}/\text{Al}_x\text{Ga}_{1-x}\text{As}$ QW samples with varying aluminum content. The results are compared with experimental electroreflectance spectra, absorption spectra simulated with multiband $\mathbf{k}\cdot\mathbf{p}$ computations, and theoretical calculations of the electronic states in the QWs. Thus, the transitions which induce steps in the SPV spectra are unambiguously identified. Most remarkably, the bound electron-to-free hole transition is detected by SPV measurements. This distinguishes the SPV method from many other optical techniques like photoluminescence and photoreflectance spectroscopy that allow only the observation of bound-to-bound and free-to-free transitions. The analogous free electron-to-bound hole transition does not give rise to a feature in the SPV spectra. In addition, the bound-to-bound transitions $e_1\text{-}hh_1$, $e_1\text{-}lh_1$, and $e_2\text{-}hh_2$ are observed, if the respective states are confined. Also, the free-to-free transition $ce\text{-}ch$ is measured. We demonstrate how these transitions can typically be identified in the spectra without any further measurements or calculations. With this knowledge, the practical band offsets of the QW structure, i.e., the energy difference between the lowest confined states in the QW and the extended states in the barrier, can be extracted directly from the spectra. An advantage over conventional techniques for the determination of band offsets is that neither any additional knowledge of other QW parameters nor simulations are necessary. As an example for the application of the SPV technique, the electronic states and band offsets of a series of $\text{In}_{0.3}\text{Ga}_{0.7}\text{As}_{0.98}\text{N}_{0.02}/\text{GaAs}$ QWs with varying QW width are characterized. These experiments directly show that nitrogen affects only the conduction band states.

DOI: [10.1103/PhysRevB.72.155324](https://doi.org/10.1103/PhysRevB.72.155324)

PACS number(s): 78.67.Lt, 78.20.Jq, 73.50.Pz, 78.55.Cr

I. INTRODUCTION

Band offsets are an important parameter of quantum well (QW) structures; and information about them is essential for the design of electronic and optoelectronic devices. Experimentally, however, band offsets are fairly difficult to determine. Conventional techniques rely on additional simulations of the QW states.¹ In turn, such simulations require good knowledge of other QW parameters like, e.g., the electron and hole effective masses. In particular for novel materials, this knowledge is not always available. For example, dilute nitrides are at present intensively investigated both because of their unusual and interesting fundamental properties and their use for optoelectronic devices.²⁻⁴ For these materials, many parameters are still unknown or not fully understood. Perhaps most eminently, the exact values of the effective masses as well as the band alignment and the band offset values are still the topic of debate.^{5,6}

Recently, we proposed a simple technique for the determination of band offsets which is based on surface photo-

voltage (SPV) measurements.^{7,8} With this method, the band offsets can be extracted directly from the spectra without the need for additional simulations or the knowledge of other parameters. For that report, we used a simple case to demonstrate that band offsets can be determined. Here, we present an extensive study that leads to a more general understanding of the SPV technique. In particular, we have found more features in the spectra for different samples, and we have unambiguously clarified which transitions they are attributed to.

SPV spectra of a series of InGaAs-QW samples have been compared with contactless electroreflectance measurements, absorption spectra simulated by the multiband $\mathbf{k}\cdot\mathbf{p}$ method, and theoretical calculations of the energy levels of the QW structures. The distinguishing feature of our SPV technique is the observation of a bound-to-free transition, namely, $e_1\text{-}ch$. The analogous transition $ce\text{-}hh_1$ does not induce a feature in the spectra. In addition, transitions between bound states ($e_1\text{-}hh_1$, $e_1\text{-}lh_1$, $e_2\text{-}hh_2$) are detected, depending on the

electronic structure of the QW (i.e., number of bound states). We illustrate how in most cases these transitions can be identified in the spectra without the help of other experimental techniques or theoretical calculations. This enables the simple extraction of the band offsets directly from the SPV spectra.

Finally, our SPV method is exemplified on a series of InGaAsN samples with varying QW width. We provide direct experimental evidence that nitrogen affects only the conduction band states. As a consequence, the redshift caused by nitrogen is larger for thicker QWs.

II. EXPERIMENTS AND SIMULATIONS

Three series of samples were used in this study. The first series consists of four In_{0.3}Ga_{0.7}As single quantum well (SQW) samples, while the second one comprises four In_{0.3}Ga_{0.7}As_{0.98}N_{0.02} SQW samples. In each series, the SQW thickness varies between 3 and 9 nm. For the samples of both of these series, the SQW is embedded in the middle of an undoped 700 nm-thick GaAs layer (barrier). The growth temperature of the SQW was about 400 °C. The third series is made up of five In_{0.15}Ga_{0.85}As/Al_xGa_{1-x}As SQW samples with the aluminum content in the barrier varying between 0% and 30%. In this case, the 9 nm-thick SQW was grown at about 500 °C inside a symmetric *n-i-p* structure: *n*-doped AlGaAs (150 nm)/undoped AlGaAs (50 nm)/undoped InGaAs (9 nm)/undoped AlGaAs (50 nm)/*p*-doped AlGaAs (150 nm). Data from a sample containing a 6.5 nm-thick In_{0.3}Ga_{0.7}As_{0.984}N_{0.016} SQW are shown as a reference at the beginning of the discussion. This sample has the structure of a laser; i.e., a 400 nm-thick GaAs layer is sandwiched between two 1.5 μm-thick AlGaAs layers that are *p* and *n* doped, respectively. Also, the SQW is surrounded by 5 nm-thick GaAs_{0.986}N_{0.014} barriers. Samples were grown by solid source molecular beam epitaxy (MBE) on *n*⁺-doped ($4 \times 10^{18} \text{ cm}^{-3}$) GaAs (001) substrates. A radio-frequency plasma source was employed to generate reactive nitrogen species from N₂.

For the SPV measurements, the sample is sandwiched between a massive copper plate (ground contact) and a transparent contact made by an indium tin oxide (ITO) layer. No dc contact is needed between the sample and the electrodes (capacitive contact). Chopped monochromatic light illuminates the sample through the ITO. The photovoltage, taken from the transparent electrode, is applied to a high impedance and analyzed by a standard lock-in technique. The capacity between the surface of the sample and the ITO couples the sample to the amplifier. By means of this ac coupling, only temporal variations of the photovoltage across the sample are measured. More details are described elsewhere.^{7,8}

The photoluminescence (PL) measurements were performed at temperatures between 15 and 300 K in a closed-cycle cryostat. The samples were excited continuously by a He-Ne laser ($\lambda=633 \text{ nm}$) with a power density of about 300 W/cm². The PL was dispersed by a single 1 m monochromator and detected by a nitrogen-cooled Ge detector.

For the contactless electroreflectance (ER) measurements we used a setup similar to that for the SPV investigations. The sample was mounted between a copper block and an ITO-coated glass plate. A $\pm 50 \text{ V}$ square wave voltage with a frequency of 339 Hz was applied to modulate the reflectance of the sample. We used a 200 W tungsten halogen lamp followed by a 32 cm monochromator and suitable glass filters as a tuneable light source. The light reflected from the sample was detected by a thermoelectrically cooled amplified InGaAs photodiode and measured simultaneously by a voltmeter and a lock-in amplifier to extract the intensity of the reflected light and its voltage-induced change from the signal, respectively.

For the analysis of the contactless ER measurements, multioscillator fits assuming a Gaussian broadening have been employed in order to extract the energetic positions of the different transitions (oscillators) from the spectra. For the quantum well transitions, the first derivative functional form (FDFF) has been applied, which is the suitable line shape for excitons in such structures. For bulk material (GaAs), the common third derivative functional form (TDFF) has been used.

In order to obtain theoretical support for our experimental results, we have simulated the energy band configuration of single quantum wells in an (Al)GaAs barrier taking into consideration both the hydrostatic and the uniaxial strain including the relevant deformation potentials. To determine the quantized states, we have used the analytical solution of the Schrödinger equation for a square well potential. In this way we have calculated the ground and the excited states (e_2, hh_2) for the QWs, taking the excitonic binding energy equal to 8 meV.⁹

The calculation of the optical absorption as a function of photon energy for interband transitions in a quantum well has been performed by means of the $8 \times 8 \mathbf{k} \cdot \mathbf{p}$ theory. The electron and hole levels and their wave functions have been calculated by using the nano device simulation tool NEXTNANO³ (Ref. 10) taking into account strain, deformation potentials, and the coupling between the conduction and valence bands. For simplicity, the exciton correction for the energy levels was neglected. From these levels, the optical absorption spectra have been calculated considering the non-parabolic $\mathbf{k} \cdot \mathbf{p}$ dispersion, i.e., also the energies and wave functions for $\mathbf{k}_{\parallel} \neq 0$.

For the N-containing structures, we have employed the band anticrossing (BAC) (Refs. 11,12) approach which was demonstrated to be a good tool (at least for the concentrations of N that we use) to describe the strong coupling between the extended conduction band states and the localized nitrogen states that characterize the dilute nitride alloys. Also in this case, the analytical solution of the Schrödinger equation for a square well potential has been employed to determine the quantized states.

III. RESULTS AND DISCUSSION

A. Optical transitions detected by surface photovoltage measurements

At first, the general principle of our method is explained as discussed in more detail earlier.^{7,8} The SPV spectrum of

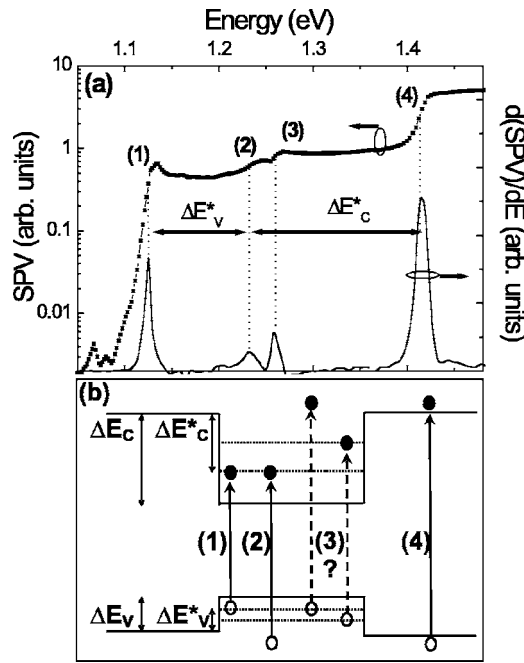


FIG. 1. (a) SPV and $d(\text{SPV})/dE$ spectra for a 9 nm-thick $\text{In}_{0.3}\text{Ga}_{0.7}\text{As}$ SQW acquired at 300 K (line with data points and solid line, respectively). (b) The possible optical transitions as discussed in Ref. 7: (1) $e_1\text{-}hh_1$ (ground state), (2) $e_1\text{-}ch$, (3) $ce\text{-}hh_1/e_2\text{-}hh_2$, and (4) $ce\text{-}ch$ (continuum).

an $\text{In}_{0.30}\text{Ga}_{0.7}\text{As}/\text{GaAs}$ single quantum well sample is presented in Fig. 1(a). The SPV signal increases with increasing energy of the incident light in four pronounced steps. The spectrum in Fig. 1(a) is qualitatively typical for many samples, but we will later show that the number of steps may differ depending on the sample structure. For a low injection of excess carriers, the SPV spectrum can be considered as an absorption spectrum.¹³ Thus, the steps therein indicate the onset of different absorption processes occurring in the sample. Figure 1(b) depicts the optical transitions that were discussed in Ref. 7 as the origin of the different steps. Transition 1 is the optical transition with the lowest possible energy, which is the transition between the bound ground states in the valence band and the conduction band of the QW ($e_1\text{-}hh_1$). Transition 2 is the transition from the extended state in the valence band to the bound state of the conduction band ($e_1\text{-}ch$). In Ref. 7, no distinction could be made between two possible origins of transition 3. As indicated in Fig. 1(b) with dashed lines, transition 3 may take place between the bound state of the valence band and the extended state of the conduction band ($ce\text{-}hh_1$). However, it may also take place between the first excited QW states ($e_2\text{-}hh_2$), i.e., between two bound states. Finally, transition 4 is the excitation of electrons from the extended states of the valence band to the extended states of the conduction band ($ce\text{-}ch$), i.e., it is due to the absorption in the GaAs barrier.¹⁴

By determining simply the differences between the energies corresponding to these optical transitions, as indicated by the double arrows in Fig. 1(a), one is able to extract the quantities ΔE_C^* and ΔE_V^* which are related to the band offsets by the expressions

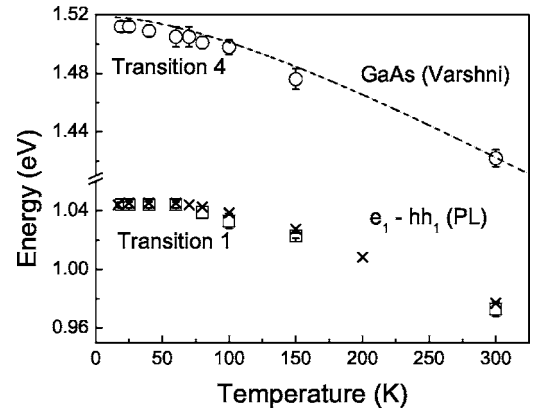


FIG. 2. Temperature dependence of the ground state (transition 1) and of the barrier (transition 4) of a 6.5 nm-thick $\text{In}_{0.3}\text{Ga}_{0.7}\text{As}_{0.984}\text{N}_{0.016}$ SQW as determined from SPV spectra (data points with error bars). Comparison of the same quantities measured with different techniques: PL for the ground state (crosses) and Varshni curve for the GaAs barrier (dashed line).

$$\Delta E_C = \Delta E_C^* + e_1,$$

$$\Delta E_V = \Delta E_V^* + h_1, \quad (1)$$

where e_1 and h_1 are the first quantized state of electrons and holes, respectively. We will call the energy quantities ΔE_C^* and ΔE_V^* “practical band offsets” (PBOs). In fact, for the operation of a real device, only ΔE_C^* and ΔE_V^* are of practical interest because they express the real carrier confinement in the QW.

In the SPV spectrum [Fig. 1(a)], the onset of the optical transitions is indicated by steps in intensity. For the precise determination of the transition energies we numerically computed the derivative of the SPV spectrum as a function of the detected energy [also shown in Fig. 1(a)].¹³ The maxima of the peaks of the derivative indicate the energy at which the steps appear, i.e., the optical transitions in the structure. All the error bars of the experimental results shown in this paper are the full widths at half maximum (FWHM) of the peaks in the derivative spectrum. Typically, the resulting precision of these measurements is about 10%.

B. First and last step in the spectra

In Fig. 2 the temperature dependence of the ground state and of the barrier of an $\text{In}_{0.3}\text{Ga}_{0.7}\text{As}_{0.984}\text{N}_{0.016}/\text{GaAs}$ SQW are compared as determined by different techniques. The data points with error bars are extracted from SPV spectra using the values of the maxima in the derivative spectra which correspond to the steps 1 and 4. The crosses show the photoluminescence (PL) peak positions of the same sample, and the dashed line the GaAs band gap as a function of temperature described by the empirical expression proposed by Varshni.¹⁵ The good agreement between the SPV data and the PL results for step 1 and the theoretical prediction for step 4 confirms the interpretation of the step 1 and 4 as described in Fig. 1(b).

C. Third step in the spectra

As already said in Sec. III A, in the paper describing our method,⁷ the interpretation of step 3 was not unambiguous. The clear distinction between e_2-hh_2 and $ce-hh_1$ as the origin of step 3 was prevented by the very small energy difference between these two transitions for that sample (less than 10 meV). In the following, we will clarify with the help of dedicated samples whether step 3 comes from a bound-to-free ($ce-hh_1$) or from a bound-to-bound transition (e_2-hh_2).

In order to elucidate the origin of step 3, a series of InGaAs samples with different QW widths have been analyzed. As all the other structural parameters remained the same, the only difference between the samples of this series is the quantization energy of the electron and hole states in the QW. While this influences all states, the effect is greater on states of higher order. Moreover, for the thinner QWs only the ground states are bound. Correspondingly, step 3 should vanish for these samples, if it is due to e_2-hh_2 .

The SPV spectra for this series are shown in Fig. 3(a). As expected, the transitions related to the GaAs barrier (step 4) have always the same energy. The experimental value of (1.42 ± 0.01) eV is in good agreement with the value of the band gap of GaAs at 300 K (1.425 eV). This is well illustrated in Fig. 3(b) where the derivative of the surface photovoltage spectra is shown. The ground state (transition 1) moves toward higher energy values for decreasing well width, since the quantization energy increases.

The position of step 3 depends also on the well width. Passing from a width of 9 to 7 nm, it moves toward higher energies and completely disappears for the samples with a QW width of 5 and 3 nm. This implies that the occurrence and the energy position of step 3 depend on the confinement of the carriers in the QW.

InGaAs/GaAs quantum wells have been studied for many years, and all the necessary material parameters are well known.¹⁶ This allowed us to simulate the energy levels of the measured $\text{In}_{0.3}\text{Ga}_{0.7}\text{As}/\text{GaAs}$ QWs with high accuracy. The simulated energies of the transitions e_1-hh_1 and e_2-hh_2 at 300 K are presented in Fig. 3(c) (solid and dashed lines, respectively). The calculated position of the transition $ce-hh_1$ is also shown (dotted line). The positions of steps 1 and 3 were extracted from the spectra in Fig. 3(b) and were also included in Fig. 3(c) (open squares and open spheres, respectively). In order to obtain a good agreement between the simulated and the experimental data for the ground state emission energy of the QW (e_1-hh_1), the conduction band offset ratio $Q_C = \Delta E_C / (\Delta E_C + \Delta E_V)$ was varied in the range of 0.6–0.7, as suggested by other groups.^{16,17}

We have obtained the best fit for $Q_C = 0.65$. Also, simulations were carried out assuming slightly different indium contents [In]. The best agreement was found for [In] = 32.5%.¹⁸ As one can see in Fig. 3(c), the resulting simulation of the transition e_2-hh_2 matches the experimental points corresponding to the transition 3. While for the 7 nm QW the experimental value could also be explained by the transition $ce-hh_1$, this is clearly not the case for the 9 nm QW. Also, if the transition $ce-hh_1$ caused a feature in the spectrum, this should occur for the QW widths 3 and 5 nm as well, which is not observed. All of this suggests that step 3 is due to the

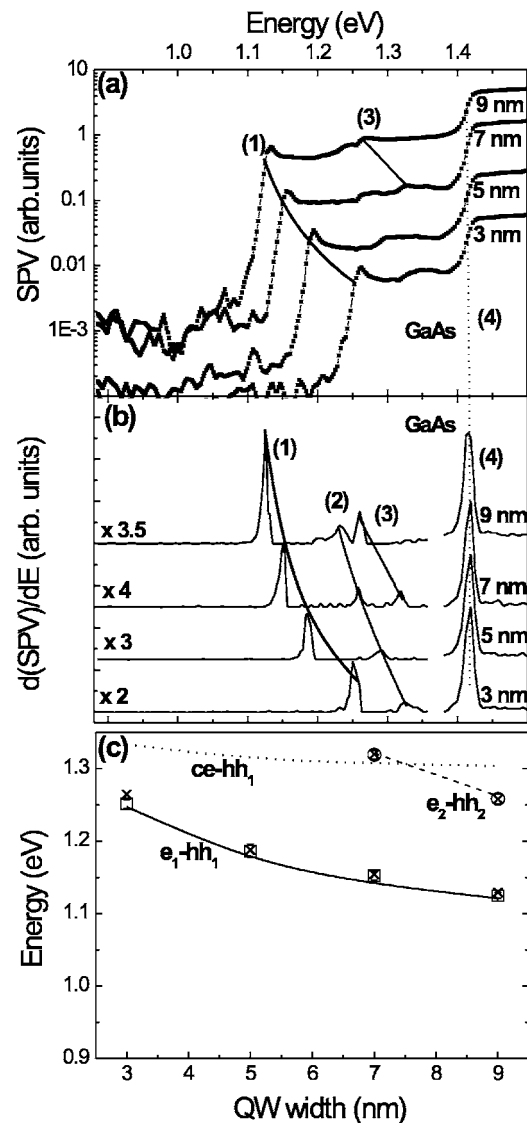


FIG. 3. (a) SPV spectra for $\text{In}_{0.3}\text{Ga}_{0.7}\text{As}$ SQWs with different well widths acquired at 300 K. The change of the position of transition 1 for different well widths is indicated by a solid line. The band gap of GaAs at 300 K is indicated by a dotted vertical line. The position of step 3 is also indicated. (b) Derivatives of the SPV spectra as a function of the detected energy. The peaks correspond to the steps in intensity of the SPV spectra. The first part of each spectrum (up to 1.38 eV) has been magnified for clarity; on the left-hand side of the curves the multiplication factors are shown. (c) Energy values of transition 1 (squares) and step 3 (spheres) in dependence of the well width. The solid and the dashed lines are the calculated values of e_1-hh_1 and e_2-hh_2 , respectively. The dotted line is the calculated value of the transition $ce-hh_1$. The small crosses are the results from the electroreflectance measurements.

transition between the first excited electron and heavy-hole states.

In order to further validate this interpretation, contactless electroreflectance measurements have been performed on the same series of samples. In Fig. 4 the experimental data (open circles) of the samples with the well widths of 7 nm (a) and 9 nm (b) are shown. The good agreement with the simulations, shown as solid lines in the figure, allows us to accu-

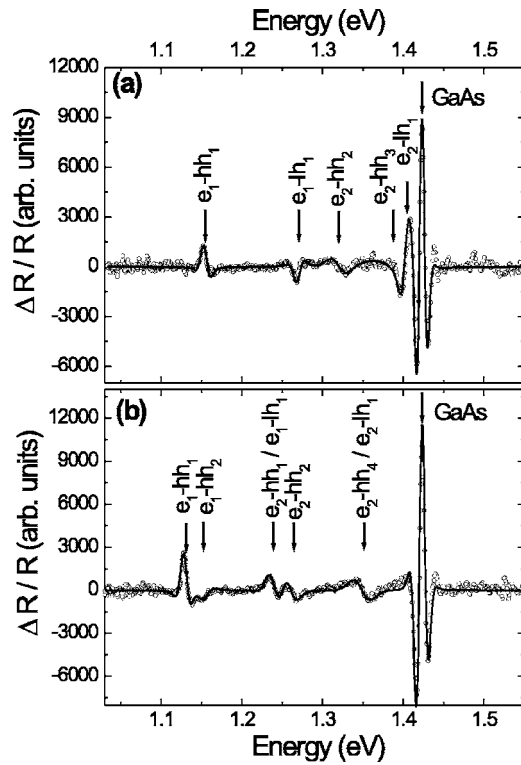


FIG. 4. Contactless electroreflectance measurements (open circles) at 300 K of a 7 nm-thick $\text{In}_{0.30}\text{Ga}_{0.70}\text{As}$ (a) and a 9 nm-thick $\text{In}_{0.30}\text{Ga}_{0.70}\text{As}$ SQW (b). The solid lines are the multi-oscillator fits which were used to determine the energetic positions of the different transitions in the QWs (indicated by arrows in the figure).

rately determine the energetic positions of the different optical transitions in the SQWs (marked by arrows). Theoretical modeling was used to identify the transitions as given in the figure. Also in this case, in order to have a good simulation, the nominal sample parameters had to be slightly modified. The indium content was assumed to be 32% and the value of the QW widths was assumed to be about 3% larger than the nominal one. In Fig. 3(c) the transitions corresponding to the ground ($e_1\text{-}hh_1$) and to the excited states ($e_2\text{-}hh_2$) extracted from the ER spectra are shown (small crosses). The excellent agreement gives us further evidence that step 3 in the SPV spectra corresponds to the transition $e_2\text{-}hh_2$.

In order to elucidate if the transition $ce\text{-}hh_1$ could give rise to a step in such SPV spectra we have simulated an absorption spectrum corresponding to the SPV spectrum shown in Fig. 1(a). For this purpose the multiband $\mathbf{k}\cdot\mathbf{p}$ method was employed without taking into account excitonic effects. We have considered the 9 nm-thick InGaAs SQW because in this case the transitions $e_2\text{-}hh_2$ and $ce\text{-}hh_1$ differ from each other by about 40 meV, as can be seen in Fig. 3(c). This offers the possibility of a clear distinction between these two transitions. In Fig. 5 the experimental SPV spectrum is shown along with the simulated absorption spectra for light propagation perpendicular to the QW along the z direction (solid line) and in the QW plane with perpendicular electric field polarization (dashed line). The calculated spectrum (x polarized) fits our experimental data quite well, which confirms the validity of our method and the conclusions regard-

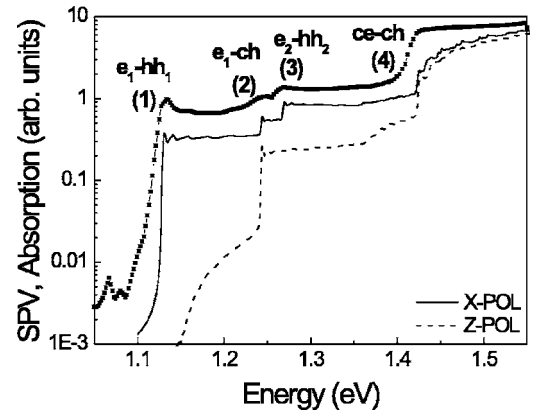


FIG. 5. SPV spectrum for a 9 nm-thick $\text{In}_{0.3}\text{Ga}_{0.7}\text{As}$ SQW acquired at 300 K (line with data points) compared with calculated (using $\mathbf{k}\cdot\mathbf{p}$ method) InGaAs absorption spectra for light propagation perpendicular to (solid line) and in the QW plane with perpendicular E-field polarization (dashed line).

ing the nature of step 3. In both the experimental and simulated spectra the transition from the bound state of the valence band to the extended state of the conduction band is absent. In the region of the spectrum where the transition $ce\text{-}hh_1$ would be expected [about 1.30 eV, see Fig. 3(c)] there is no variation in intensity. In conclusion of this section, step 3 in the SPV spectra is caused by the bound-to-bound transition $e_2\text{-}hh_2$, and the bound-to-free transition $ce\text{-}hh_1$ does not induce any step.

D. Second step in the spectra

In Ref. 7, the nature of step 2 was analyzed partly with the help of a QW transmission spectrum for in-plane light propagation and perpendicular electric field polarization. For this geometry, only optical transitions involving light holes are allowed. Since the transmission decreased at the position of step 2 and since light holes were not confined in the respective QW, step 2 was associated with the transition $e_1\text{-}ch$. An analogous behavior can be seen in Fig. 5. The z -polarized curve corresponds to the absorption in transverse magnetic mode (TM) for which only transitions involving light hole can contribute. In our structures the energy level of the light holes lies within a few milli-electron-volts to the valence band energy. For this reason, the onset of the absorption in the z -polarized mode must occur in the immediate proximity of the step attributed to $e_1\text{-}ch$, as it is indeed the case in Fig. 5.

All the samples investigated until now have the peculiarity that the light-hole energy level is located very close to the valence band edge of the QW barrier. Hence, step 2 in the SPV spectra could possibly have been caused by a transition between e_1 and the lightly bound level lh_1 . This could mean that possibly bound-to-free transitions might not be observable at all. In order to clarify this uncertainty, we have studied a series of samples for which the light hole level changes from free to bound.

The SPV spectra of $\text{In}_{0.15}\text{Ga}_{0.85}\text{As}/\text{Al}_x\text{Ga}_{1-x}\text{As}$ SQW samples with $0 < x < 0.3$ are shown in Fig. 6(a). The deriva-

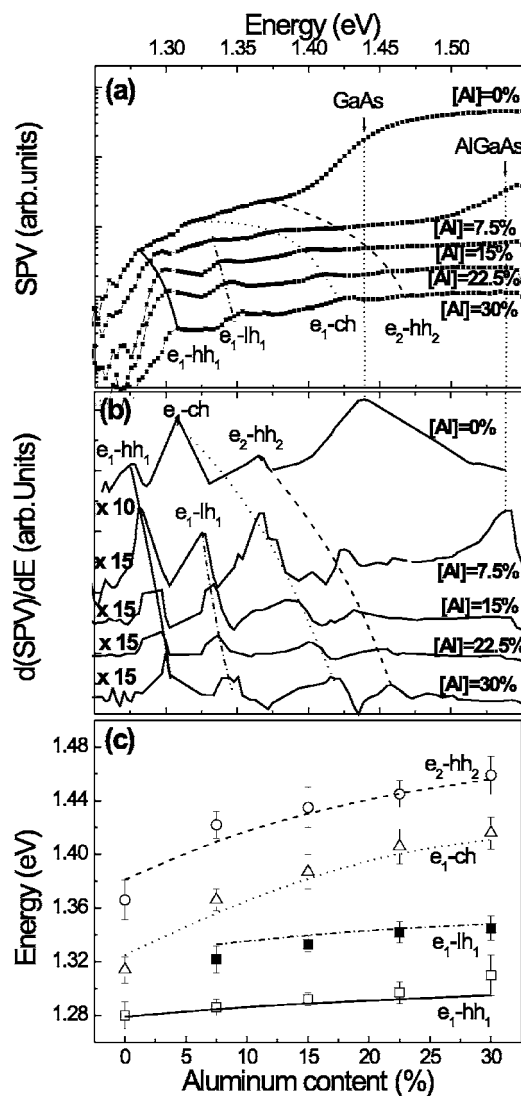


FIG. 6. (a) SPV spectra for 9 nm-thick $\text{In}_{0.15}\text{Ga}_{0.85}\text{As}/\text{Al}_x\text{Ga}_{1-x}\text{As}$ SQWs with different aluminum content in the barrier ($0 < x < 0.3$) acquired at 275 K. The optical transitions visible in the spectra are indicated with different lines as guides for the eye: solid line (e_1-hh_1), dotted-dashed line (e_1-lh_1), dotted line (e_1-ch), and dashed line (e_2-hh_2). The band gap of the barrier GaAs and of the barrier $\text{Al}_{0.075}\text{Ga}_{0.0925}\text{As}$ at 275 K are indicated by a dotted vertical line. (b) Derivatives of the SPV spectra as a function of the detected energy. The peaks correspond to the steps in intensity of the SPV spectra. The first part of each spectrum has been magnified for clarity; on the left-hand side of the curves the multiplication factors are shown. (c) Experimental points of the energy transitions extracted by the SPV spectra in the function of the aluminum content. The solid, the dotted-dashed, the dotted, and the dashed lines are the calculated values of the transitions e_1-hh_1 , e_1-lh_1 , e_1-ch , and e_2-hh_2 , respectively.

tives of the spectra are shown in Fig. 6(b). As expected, the position of the step on the right-hand side of the spectrum, which is attributed to the transition in the barrier ($ce-ch$), moves to higher energies as the aluminum content in the barrier is increased from 0% to 7.5%. For higher aluminum contents, this step is located beyond the range of energies accessible to our experimental setup. Most notably, the pres-

ence of aluminum in the barrier gives rise to an additional step (indicated by a dotted-dashed line in the figure) close to the one related to the transition e_1-hh_1 (solid line). Thus, there are altogether five steps in the spectrum. It is known that light holes are not confined for an $\text{In}_{0.15}\text{Ga}_{0.85}\text{As}/\text{GaAs}$ structure.¹⁷ Adding more and more Al to the barrier, the carrier confinement increases and the light holes become bound. This suggests that the additional step is related to bound light holes, with the transition e_1-lh_1 being the most likely candidate.

Again, the relevant QW states were simulated in order to verify the nature of the different steps. The results of these simulations are displayed in Fig. 6(c) along with the experimental values for the first four steps in the spectra. The good agreement confirms that the additional step is caused by the transition e_1-lh_1 .

It is important to stress here that independent of the presence of the other steps, the transition e_1-ch induces a step in the spectrum *in any case*. This is a fundamental feature for our method on the basis of which one is always able to determine the band offsets of the structure, provided that bound-to-free transition e_1-ch can be identified with one of the steps in the spectrum. This will be discussed in more detail in Sec. III F.

E. Refined interpretation of the surface photovoltage spectra

We have shown that our SPV spectra are characterized by different steps which correspond to different optical transitions in the QW. We have recognized these transitions as bound-to-bound

($e_1-hh_1, e_1-lh_1, e_2-hh_2$), bound-to-free (e_1-ch), and free-to-free transitions ($ce-ch$). This is well described by the spectrum of the sample with $[\text{Al}] = 7.5\%$ in the barrier which contains all the mentioned transitions above [see Fig. 7(a)]. These optical transitions are indicated in Fig. 7(b). Passing from low to higher energies, the first step (1) is clearly associated to the absorption of the ground state (e_1-hh_1). The last one (5) is, without doubt, related to the absorption in the barrier. We have demonstrated that between these two steps the transition from the extended state of the valence band to the bound state in the conduction band (e_1-ch) (3) can always be detected. The observation of this bound-to-free transition distinguishes our SPV method from many other techniques like PL or photoreflectance (PR) and enables the easy determination of band offsets, as will be discussed in more detail later. Depending on the sample structure, the bound-to-bound transitions e_1-lh_1 (2) and e_2-hh_2 (4) generate steps in the SPV spectrum. Further bound-to-bound transitions could also generate steps if the QW contains more bound states.

In our spectra we have not seen bound-to-free transitions other than e_1-ch . Transitions involving the conduction extended states and valence confined states (e.g., $ce-hh_1, ce-lh_1, ce-hh_2$) do not seem to generate any step in the SPV spectra, at least with our sensitivity and resolution. This suggests that these transitions are very weak. The above finding is in accord with a previous report. Ksendzov *et al.*,¹⁹ employing polarization-modulated absorption measurements for

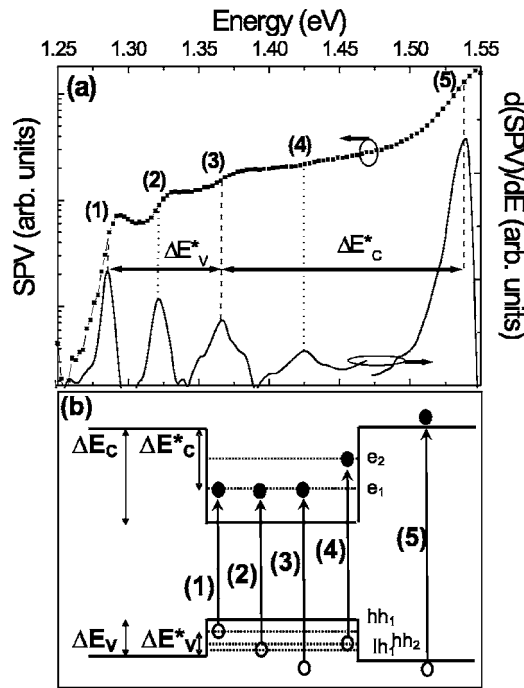


FIG. 7. (a) SPV and $d(\text{SPV})/dE$ spectra for a 9 nm-thick $\text{In}_{0.15}\text{Ga}_{0.85}\text{As}/\text{Al}_{0.075}\text{Ga}_{0.925}\text{As}$ SQW acquired at 275 K. (b) Schematic drawing of the optical transitions visible in the spectrum: (1) $e_1\text{-hh}_1$, (2) $e_1\text{-lh}_1$, (3) $e_1\text{-ch}$, (4) $e_2\text{-hh}_2$, and (5) $ce\text{-ch}$ (continuum).

an $\text{In}_{0.25}\text{Ga}_{0.75}\text{As}/\text{GaAs}$ SQW structure, have shown a strong difference in intensity between the bound-to-free transitions involving the confined electrons or the confined holes states. In particular, in their absorption spectra only the $e_1\text{-ch}$ transition generates a clear step in intensity. Although they do not give any explanation for that, they found that the geometry of the structures can influence the step intensity. In a calculation, they demonstrated that increasing the number of the wells in the sample one is able to improve the steplike feature in an absorption spectrum derived from a bound-to-free transition and, in this way, improve the intensity of the weakest transitions. Further investigations are necessary in order to verify this point.

F. Determination of the band offsets

Band offsets of a QW structure are not simple to measure. The majorities of the electronic and optical methods are indirect and, in order to give reasonable results, need the support of simulations.¹ For such simulations it is necessary to know accurately the parameters of the structures. This is not always possible, especially for some particular materials like the dilute nitrides for which many fundamental parameters still remain unknown.

The main advantage of our method is the possibility to determine the value of the band offsets (in first approximation considering the practical band offsets) of a QW structure simply by analyzing a SPV spectrum. The basis of this possibility is the fact that, in contrast to most other techniques like PL, excitation photoluminescence (PLE) and PR, a bound-to-free transition induces a clear feature in the SPV

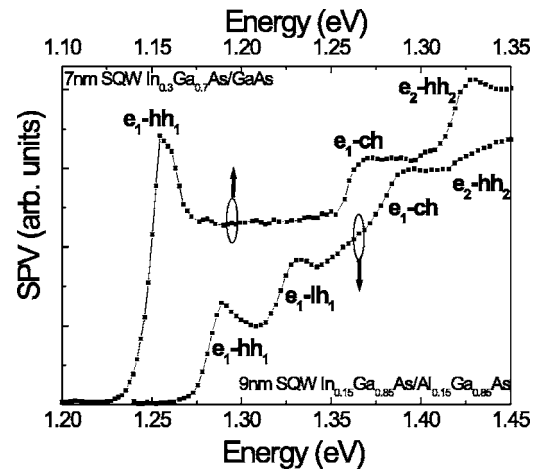


FIG. 8. SPV spectra of a 7 nm-thick $\text{In}_{0.3}\text{Ga}_{0.7}\text{As}/\text{GaAs}$ SQW sample and a 9 nm-thick $\text{In}_{0.15}\text{Ga}_{0.85}\text{As}/\text{Al}_{0.15}\text{Ga}_{0.85}\text{As}$ SQW sample taken at 300 K. The transitions $e_1\text{-hh}_1$ and $e_1\text{-lh}_1$ show excitonic features. This helps to identify the position of the step $e_1\text{-ch}$. Note that the two spectra are shifted in energy by 100 meV from each other.

spectra. The only difficulty consists in the exact identification of the steps in the spectrum without employing any type of simulation or calculation to determine the energy states of the structure. In particular, the identification of the transitions related to the ground state and to the barrier as well as of the bound-to-free transition $e_1\text{-ch}$ is fundamental for the determination of the band offsets. The former two transitions are easily found as the first and last steps in the spectrum. Thus, the crucial point is to identify the transition from the electron bound state to the extended valence state ($e_1\text{-ch}$).

We have seen that for QW structures with $\Delta E_C > \Delta E_V$, with a well width less than 10 nm and with a type I band configuration, $e_1\text{-ch}$ is the first step at energies above the step corresponding to the transition $e_1\text{-hh}_1$ (Fig. 3). However, if the light hole levels are bound in the QW, this rule does not apply any more because in this situation a step corresponding to the transition $e_1\text{-lh}_1$ appears between the steps related to the transitions $e_1\text{-hh}_1$ and $e_1\text{-ch}$, respectively (Fig. 6). In this case, however, the excitonic enhancement characteristic for the two ground states can be used as the discerning element. An example is shown in Fig. 8 in which the SPV spectra of an $\text{In}_{0.3}\text{Ga}_{0.7}\text{As}/\text{GaAs}$ SQW and of an $\text{In}_{0.15}\text{Ga}_{0.85}\text{As}/\text{Al}_{0.15}\text{Ga}_{0.85}\text{As}$ SQW are compared. The excitonic features of the ground states $e_1\text{-hh}_1$ and $e_1\text{-lh}_1$ are clearly visible in the spectra. Therefore a guiding rule could be that $e_1\text{-ch}$ is associated with the first step at energies above the ground state without excitonic enhancement.

In an unknown sample with arbitrary type I band offsets and unknown well width, SPV measurements alone cannot be used unambiguously to identify the nature of all the steps present in the spectra. In this case, additional optical investigations (e.g., PLE or ER) are necessary in order to identify the bound-to-bound transitions characteristic for that structure and to recognize in the SPV spectrum the transition $e_1\text{-ch}$ required to calculate the practical band offsets.

Once the bound-to-free transition $e_1\text{-ch}$ is identified, the practical band offsets ΔE_V^* and ΔE_C^* can easily be extracted

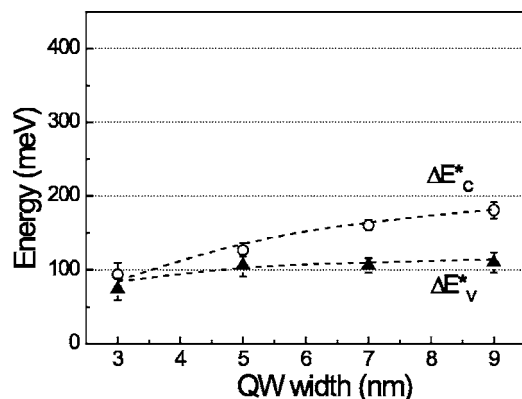


FIG. 9. Experimental values of the practical band offsets ΔE_C^* and ΔE_V^* extracted from the SPV spectra of $\text{In}_{0.3}\text{Ga}_{0.7}\text{As}$ SQWs as a function of the well width. The dashed lines are the theoretical simulations of the same quantities.

from the SPV spectra simply by determining the differences between the energetic positions of the steps related to the transitions e_1-hh_1 and e_1-ch , and e_1-ch and $ce-ch$, respectively [see Fig. 1(a)]. In the $\text{InGaAs}/\text{GaAs}$ SQW thickness series (Fig. 3) for example, these transitions correspond to the steps 1, 2, and 4. This is not the case for the $\text{InGaAs}/\text{AlGaAs}$ [Al] series (Fig. 6), for which the detection of the transition $ce-ch$ was in most cases prevented by the limitations of our experimental setup: only signals up to 1.55 eV could be detected.

As shown in Fig. 2, SPV measurements can be taken at different temperatures, thus in principle, it is possible to study the evolution of the band offsets with temperature. On the other hand, as described in Ref. 7, the SPV intensity of the different steps varies with temperature. In particular, it strongly decreases with decreasing T , making the band offsets determination extremely complicated and in some cases impossible to realize. A detailed analysis of applying the SPV technique at different temperatures is beyond the scope of this work.

From the derivatives of the SPV spectra in Fig. 3(b), we have extracted the practical band offsets of the $\text{InGaAs}/\text{GaAs}$ series and we have plotted them, as a function of the well width, in Fig. 9. The experimental data points show an increase of both ΔE_C^* and ΔE_V^* with increasing well width. Since the band offsets remain unchanged, this increase is due only to the decrease in energy of the values of the first quantized state for electrons and holes. Using again the value of $Q_C=0.65$ and the other structural parameters described above, the PBOs were simulated (dashed lines in Fig. 9). The very good agreement between the experimental data and the simulations confirms that what we can extract from the surface photovoltage spectra is exactly the energy difference between the conduction (valence) band offset and the first quantized energy state of electrons (holes).

G. Comparison with other techniques

It is well known that the energy dependence of the density of states of a QW leads to a staircaselike absorption spectrum for the transitions between confined states.²⁰ However, little

attention has been paid to the effects of transitions between confined and extended states on the absorption spectra. Different groups,^{19,21} employing different experimental techniques (PLE, PR), have shown the possibility to detect bound-to-free transitions. The majority of the experiments were performed on multiquantum well structures and it was shown that the contribution of these transitions was small compared to the contribution of the transitions between confined states. It should be noted here that the use of multi-QW samples is not always possible due to strain considerations. In one case for a SQW sample,¹⁹ however, employing polarization-modulated absorption measurements, it was shown that bound-to-free transitions have the same strength and produce the same steplike absorption features as bound-to-bound transitions, at least for the transition e_1-ch . Nevertheless in this reference, the data in the spectra were reliable only up to the energy position of the first excited state. At that point, in fact, the strong absorption in the substrate prevented the possibility to detect other transitions inside the SQW.

In contrast to this, SPV has the advantage to allow the detection of *all* bound-to-bound transitions *and also* of bound electron-to-free hole transitions, with high sensitivity even in single quantum well samples. Bound-to-bound transitions must be intended here between subbands of the same order (e.g., e_1-hh_1 , e_1-lh_1 , e_2-hh_2, \dots). Transitions between subbands of different order (e.g., e_1-hh_2 , e_2-hh_3, \dots) do not generate any step in our SPV spectra.

Compared to photoluminescence spectroscopy that gives clear information only about the first quantum transition (the excited states can be detected only with a large excitation power density), SPV spectra easily resolve transitions between excited states in the QW. Further advantages of our measurement technique are the simple experimental setup compared to other optical measurement techniques like PLE and the fact that the samples must not be subject to special treatments (e.g., thinning process for some cases in the transmission spectroscopy). Moreover, the simple structure of the samples employed in our measurements allows the simulation of the energy levels in the QW with high accuracy.

Our results show that simply by employing SPV it is possible to obtain comprehensive information about SQWs which otherwise could be achieved only by combining different optical techniques and theoretical calculations.

H. Effect of N on the band structure of InGaAs

With our results we have shown that from the SPV spectrum, the transitions between the ground and the excited states in the QW and the practical band offsets can be extracted at the same time. Thus, by measuring the SPV spectra of a small series of samples the influence of different QW parameters on both the conduction and valence band states can be studied. This will be exemplified in the following. Another application of the SPV technique can be found in a recent work in which the influence of the nitrogen and indium content on the band offsets of $\text{InGaAsN}/\text{GaAs}$ SQW samples has been described.²²

SPV measurements were performed on a series of $\text{InGaAsN}/\text{GaAs}$ SQW samples with different well width.

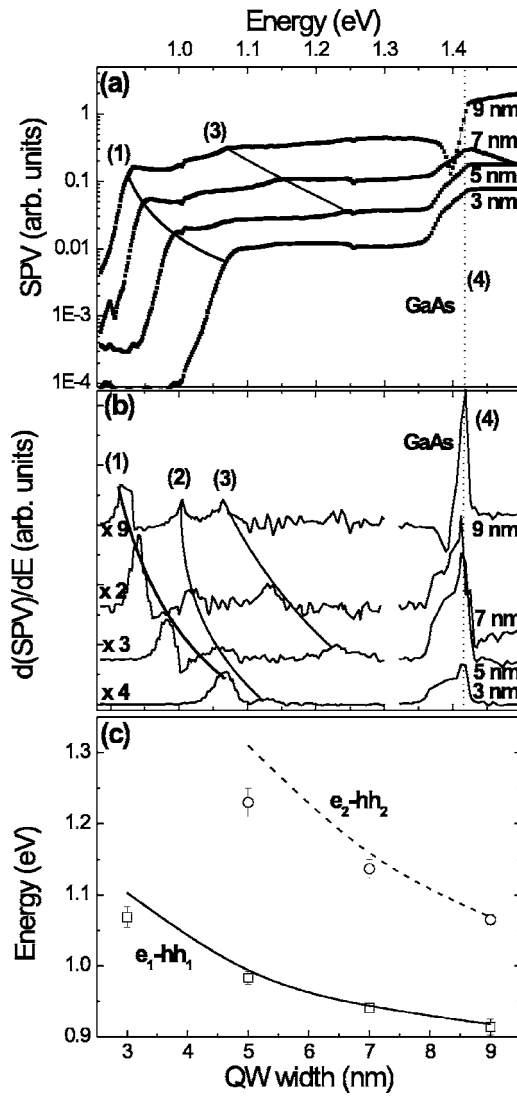


FIG. 10. (a) SPV spectra for $\text{In}_{0.3}\text{Ga}_{0.7}\text{As}_{0.098}\text{N}_{0.02}$ SQWs with different well widths acquired at 300 K. The different positions of transition 1 for different well widths are indicated by a solid line. The fixed position of the barrier (GaAs) is indicated with a dotted vertical line. The presence of step 3 is also indicated. (b) Derivatives of the SPV spectra as a function of the detected energy. The peaks correspond to the steps in intensity of the SPV spectra. The first part of each spectrum (up to 1.30 eV) has been magnified for clarity; on the left-hand side of the curves the multiplication factors are shown. (c) Energy values of transitions 1 (squares) and 3 (spheres) in dependence of the well width. The solid and the dashed lines are the calculated values of $e_1\text{-}hh_1$ and $e_2\text{-}hh_2$, respectively.

The spectra are shown in Fig. 10(a). The derivatives of these spectra make the identification of the different steps easier and are shown in Fig. 10(b). The SPV spectra of InGaAsN exhibit an increased noise level compared to the analogous spectra of InGaAs in Fig. 3(a). This finding is attributed to the reduced crystal quality. Also, in the GaAs absorption region above 1.38 eV the 7 and 9 nm-thick samples show an unusual behavior. At the moment, we do not have a clear explanation for this phenomenon but similar spectra have been reported before.²³ As for the InGaAs/GaAs samples, the ground state energy value (transition 1) increases with

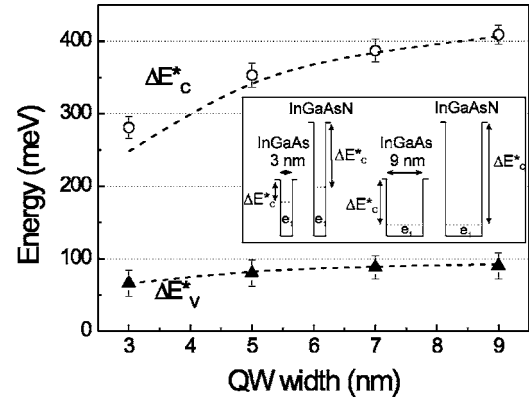


FIG. 11. Experimental values of the practical band offsets ΔE_C^* and ΔE_V^* extracted from the SPV spectra of $\text{In}_{0.3}\text{Ga}_{0.7}\text{As}_{0.098}\text{N}_{0.02}$ SQWs as a function of the well width. The dashed lines are the theoretical simulations of the same quantities. In the inset the influence of the well width on the structure of the electron states of $\text{In}_{0.3}\text{Ga}_{0.7}\text{As}$ and $\text{In}_{0.3}\text{Ga}_{0.7}\text{As}_{0.098}\text{N}_{0.02}$ SQWs is shown. For illustrative purposes, the bottoms of the QWs are aligned. In reality, the energetic level of the GaAs barrier is the same for all the QWs.

decreasing well width and the transition corresponding to the barrier has the same value for all the samples. The energy position of step 3, that was extensively discussed for the series of InGaAs samples and that is attributed to the transition $e_2\text{-}hh_2$, varies with the well width here as well. In this case, however, it is possible to detect this transition also for the sample having a well width of 5 nm. Since the presence of nitrogen reduces the band gap energy of the QW compared to InGaAs, thus increasing the carrier confinement, it is reasonable that bound excited states occur for smaller well widths.

The energetic positions of the steps (1) and (3) are depicted in Fig. 10(c) versus the QW width and are marked with open squares and open spheres, respectively. The comparison of Figs. 3(c) and 10(c) reveals the influence of nitrogen on the energetic states in the QW. The incorporation of 2% of nitrogen into InGaAs generates a redshift of the transition of the confined QW states $e_1\text{-}hh_1$ of about 200 meV. In particular, passing from the 3 to 9 nm-thick samples, the redshift increases from 185 to about 215 meV, showing thus a dependence on the QW width. The excited states, corresponding to the transition $e_2\text{-}hh_2$, show the same trend. The influence of the well width will be explained below. The average redshift of roughly 200 meV is in line with other studies that state an energy gap reduction rate of about 100 meV per percent of nitrogen.^{2,11}

The values of the conduction and valence practical band offsets were extracted from the SPV spectra depicted in Figs. 10(a) and 10(b) and are shown in detail in Fig. 11. The comparison with Fig. 9 gives us the additional possibility to distinguish between the effect of nitrogen on the conduction and on the valence band. While the valence practical band offsets assume almost the same values in both series of samples (between 75 and 110 meV for well widths between 3 and 9 nm), the values of ΔE_C^* for the InGaAsN samples are remarkably greater than the ΔE_C^* values for the N-free samples. This is direct experimental evidence that in In-

GaAsN alloys nitrogen affects mostly the electronic structure of the conduction band states and leaves the valence band states nearly unaltered. This conclusion is in accord with theoretical models about the influence of N on the band structure of InGaAsN alloys.^{11,24} A close inspection of Figs. 9 and 11 reveals for InGaAsN a slight decrease in the values of the valence practical band offset for the same well width. This is attributed to the reduction in strain by the incorporation of nitrogen. Thereby, the splitting of the two hole subbands is decreased and, hence, the PBO as well.

The comparison of the two QW width series yields another interesting result that has been mentioned already above. Apparently, the variation of e_1-hh_1 with the well width is significantly stronger for the nitrogen-containing samples. Passing from 3 to 9 nm-thick QWs, the change of e_1-hh_1 is about 125 meV in the case of InGaAs but about 155 meV for InGaAsN, as can be seen from the comparison of the experimental data in Figs. 3(c) and 10(c). In other words, the redshift induced by the incorporation of N depends on the well width. The comparison of Fig. 9 and 11 shows that the origin of this phenomenon must be related to the conduction band states. The presence of nitrogen in the InGaAsN samples increases the conduction band offset remarkably. This leads to an enhancement of the quantum well confining potential, whose influence on the confined states depends on the width of the QW. The evolution of the electron quantized states for the two extreme well widths is illustrated in the inset of Fig. 11 for both InGaAs and InGaAsN. Since we have shown that nitrogen influences mostly the conduction band, we discuss here only the case of the electron states. While for the 3 nm-thick QW the incorporation of 2% of nitrogen produces an increase of the energy value of the quantized state e_1 of about 40%, for the 9 nm-thick QW e_1 remains almost unchanged. This means that, although the change in the conduction band offset is the same, the increase of the practical band offset is stronger for the samples with a wider QW. For the 3 nm-thick QW sample the value of ΔE_C^* increases by about 175 meV, while for the 9 nm-thick QW sample the same quantity increases by about 230 meV.

Properties like that are of great interest for the design of quantum well devices. For the high-temperature performance of a quantum well laser, for example, a large practical band offset is desirable. At the same time, the degradation of InGaAsN with increasing nitrogen content suggests that as long wavelengths as possible should be reached with as little nitrogen as possible. Both findings imply the use of thick QWs. However, these results need to be balanced with strain considerations and the dependence of gain on the QW width.

In addition to the extraction of PBOs directly from the SPV spectra, we have again simulated the QW states and PBOs. The comparison of the experimental data and simulation enables us to determine indirectly important material parameters of dilute nitrides. This will be explained in the following.

Due to the highly localized nature of the perturbation introduced by the N atoms, it is not possible to use the same theoretical methods as for the N-free structures in order to predict the energy levels. For this reason the band anticrossing model¹¹ was employed for our calculations. This model consists of two interacting energy levels, one at the energy

E_M associated with the extended conduction band edge states of the (In)GaAs matrix, and the other one at energy E_N associated with the localized N impurity states. The interaction between these two levels is described by a matrix element $V_{NM}=C_{NM}\sqrt{y}$, where C_{NM} is the band interaction parameter and y is the nitrogen concentration. This interaction leads to a characteristic splitting of the conduction band into two nonparabolic subbands. For $\mathbf{k}=0$, the energies of the subbands for InGaAsN QW structures can be expressed as

$$E_{\pm}(\text{In}_x\text{Ga}_{1-x}\text{As}_{1-y}\text{N}_y) = \frac{E_M(x) + E_N \pm \sqrt{[E_M(x) - E_N]^2 + 4V_{NM}^2(x,y)}}{2}. \quad (2)$$

In addition, the electron effective mass can be approximated as²⁵

$$\frac{1}{m_e^*} = \frac{1}{2m_M} \left[1 - \frac{E_M - E_N}{\sqrt{(E_M - E_N)^2 + 4V_{NM}^2}} \right], \quad (3)$$

where m_M is the effective mass of the InGaAs ternary compound (E_M band near $\mathbf{k}=0$). Taking into account the indium dependence of the nitrogen impurity level, we have employed the following expression to calculate E_N :²⁶

$$E_N(x) = 1.65(1-x) + 1.44x - 0.38x(1-x). \quad (4)$$

As in the case of the N-free samples, the calculations of the energy levels in the InGaAsN samples were performed assuming [In]=32.5%. In this way it is possible to calculate the band gap of the quaternary material and then, by solving the Schrödinger equation for a square well potential, the quantized states in the QW.

In Fig. 10(c), the simulations of e_1-hh_1 and e_2-hh_2 are shown (solid and dashed lines, respectively). For the ground states, experimental data and simulation are in agreement. However, for the transition e_2-hh_2 the agreement is not as good, in particular at the smallest well width of 5 nm. This effect can be explained by the strongly nonparabolic dispersion of the InGaAsN conduction band, which was not considered in our calculations of the confined states. This nonparabolicity affects mostly the quantization energies for the conduction band states with high values of the wave vector \mathbf{k} (e.g., excited conduction band states).

In Fig. 11 the theoretical simulations of the practical band offsets for the InGaAsN samples are shown (dashed lines). Also in this case, there is a good agreement between the simulations and the experimental data. For these calculations, we have slightly varied the conduction band offset ratio around the value of 80% which is the value that several groups^{27,28} reported for InGaAsN SQWs with an indium content of about 30% and a low nitrogen concentration (<2%). We have obtained good results for $Q_C=0.82$. Taking also C_{NM} as an adjustable parameter in our calculations, we have achieved a good agreement between simulation and experimental data for $C_{NM}=2.36$ eV. In the literature it is possible to find different energy values between 1.35 and 3.2 eV (Ref. 29) for the parameter C_{NM} in $\text{In}_x\text{Ga}_{1-x}\text{As}_{1-y}\text{N}_y$ structures. Our C_{NM} is consistent with values reported by the majority of the groups^{12,30,31} which believe that in InGaAsN

structures C_{NM} assumes a value smaller than 2.7 eV, which is the accepted value for In-free GaAs_{1-y}N_y structures.³²

Finally, employing Eq. (3), the value of $m_e^* = 0.063 m_0$ was found for the electron effective mass. While this value is consistent with the calculated results presented by Hèroux *et al.* (In_{0.15}Ga_{0.85}As_yN_{1-y} SQWs),¹² it seems to be slightly below the experimental values reported by other groups.^{27,28,33}

IV. CONCLUSIONS

In order to generalize the understanding of the number and the kind of optical transitions that can be detected by surface photovoltage measurements in type I QW structures, we carried out an extensive study on specially designed samples. As a well-understood reference, we used InGaAs/(Al)GaAs SQWs in which the thickness of the SQWs and the aluminum content in the barrier were systematically varied to modify the confinement of the electron and the hole states. SPV spectra of SQW samples with suitable structure are characterized by several steps in intensity that indicate the energies of different optical transitions. For the unambiguous identification of these transitions, we have compared the SPV results with experimental electroreflectance spectra, absorption spectra simulated with multiband $\mathbf{k} \cdot \mathbf{p}$ computations, and theoretical calculations of the electronic states in the SQWs.

Most importantly, a bound-to-free transition, namely, e_1 - ch , can be measured with the SPV technique. A step in the spectra corresponding to the analogous transition ce - hh_1 is not found. In addition, the bound-to-bound transitions e_1 - hh_1 , e_1 - lh_1 , e_2 - hh_2 are observed, if the respective states are confined in the QW. Also, the free-to-free transition ce - ch (absorption in the barrier) is detected. The simultaneous

observation of both the bound-to-free transition e_1 - ch , the bound-to-bound transition e_1 - hh_1 , and the free-to-free transition ce - ch enables the direct determination of practical band offsets from the SPV spectra. (The practical band offsets differ from the conventional band offsets by the quantization energies of the ground states.) We have illustrated how these transitions can in most cases be identified in the SPV spectra without the need for additional experiments or simulations.

Compared to many other optical techniques (e.g., photoluminescence, photoluminescence excitation, photoreflectance spectroscopy), the SPV method stands out by allowing the simultaneous measurement of a greater variety of transitions, and in particular of a bound-to-free one. An important advantage over conventional ways to determine band offsets is that neither the knowledge of other QW parameters nor complementing simulations are necessary. In contrast to absorption spectroscopy, the sensitivity of the SPV technique is so high that even single quantum well samples can be easily characterized. At the same time, the experimental setup for SPV measurements is fairly simple. Therefore, the SPV method studied in this report is an extremely versatile and useful technique to characterize the electronic structure of QW samples.

To illustrate the usefulness of our SPV technique, we have presented the study of the influence of nitrogen on the electronic structure of InGaAs QWs. These measurements provided direct experimental evidence that nitrogen affects mostly the conduction band states and leaves the valence band basically unchanged. The incorporation of 2% nitrogen modifies the conduction band offset ratio Q_C from a value of 65% for In_{0.3}Ga_{0.7}As samples to a value of 82% for In_{0.3}Ga_{0.7}As_{0.98}N_{0.02} samples. A consequence of the exclusive effect on the conduction band is that the redshift induced by the incorporation of nitrogen is larger for thicker QWs.

*Electronic mail: massimo.galluppi@infineon.com

¹J.-P. Reithmeier, R. Höger, H. Riechert, A. Heberle, G. Abstreiter, and G. Weimann, *Appl. Phys. Lett.* **56**, 536 (1990); G. Ji, D. Huang, U. K. Reddy, H. Unlu, T. S. Henderson, and H. Morkoç, *J. Vac. Sci. Technol. B* **5**, 1346 (1987).

²For reviews see, e.g., I. A. Buyanova, W. M. Chen, and B. Monemar, *MRS Internet J. Nitride Semicond. Res.* **6**, 2 (2001); M. Hetterich, in *GaInNAs: Fundamentals of a New Material System for Near-Infrared Optoelectronics*, edited by H. Kalt and M. Hetterich (Springer, Berlin, 2004), pp. 275–288.

³M. Kondow, K. Uomi, A. Niwa, T. Kitatani, S. Watahiki, and Y. Yazawa, *Jpn. J. Appl. Phys., Part 1* **35**, 1273 (1996).

⁴H. Riechert, A. Ramakrishnan, and G. Steinle, *Semicond. Sci. Technol.* **17**, 892 (2002).

⁵J. B. Hèroux, X. Yang, and W. I. Wang, *J. Appl. Phys.* **92**, 4361 (2002) and references therein.

⁶I. A. Buyanova, G. Pozina, P. N. Hai, W. M. Chen, H. P. Xin, and C. W. Tu, *Phys. Rev. B* **63**, 033303 (2001); P. Krispin, S. G. Spruytte, J. S. Harris, and K. H. Ploog, *J. Appl. Phys.* **88**, 4153 (2000); T. Kitatani, M. Kondow, T. Kikawa, Y. Yazawa, M. Okai, and K. Uomi, *Jpn. J. Appl. Phys., Part 1* **38**, 5003 (1999).

⁷Gh. Dumitras, H. Riechert, H. Porteanu, and F. Koch, *Phys. Rev. B* **66**, 205324 (2002).

⁸Gh. Dumitras and H. Riechert, *J. Appl. Phys.* **94**, 3955 (2003).

⁹J. P. Reithmaier, R. Höger, and H. Riechert, *Phys. Rev. B* **43**, 4933 (1991).

¹⁰The NEXTNANO³ software package can be downloaded from www.wsi.tum.de/nextnano3 and www.nextnano.de

¹¹W. Shan, W. Walukiewicz, J. W. Ager III, E. E. Haller, J. F. Geisz, D. J. Friedman, J. M. Olson, and S. R. Kurtz, *Phys. Rev. Lett.* **82**, 1221 (1999); A. Lindsay and E. P. O'Reilly, *Solid State Commun.* **112**, 443 (1999).

¹²J. B. Hèroux, X. Yang, and W. I. Wang, *J. Vac. Sci. Technol. B* **20**(3), 1154 (2002).

¹³L. Kronik and Y. Shapira, *Surface Photovoltage Phenomena: Theory, Experiment, and Applications* (Elsevier, Amsterdam, 1999).

¹⁴It should be mentioned that in Ref. 8, transition 3 was assumed to originate from a bound-to-extended state transition. In the following we will show that the assumption is generally incorrect, which means that transition 3 cannot be used for the determination of the band offsets. The values obtained in Ref. 8 are correct

- because coincidentally the energies of two possible transitions are identical.
- ¹⁵Y. P. Varshni, *Physica (Utrecht)* **34**, 149 (1967).
 - ¹⁶D. J. Arent, K. Deneffe, C. van Hoff, J. De Boeck, and G. Borghs, *J. Appl. Phys.* **66**(4), 1739 (1989); G. Ji, D. Huang, U. K. Reddy, T. S. Henderson, R. Houdré, and H. Morkoç, *ibid.* **62**, 3366 (1987); J. Micallef, E. H. Li, and B. L. Weiss, *Superlattices Microstruct.* **13**, 125 (1993); I. Vurgaftman, J. R. Meyer, and L. R. Rom-Mohan, *J. Appl. Phys.* **89**, 5815 (2001)
 - ¹⁷J.-Y. Marzin, M. N. Charasse, and B. Sermage, *Phys. Rev. B* **31**, 8298 (1985).
 - ¹⁸The deviation from the nominal value is explained by the fact that the ion gauge monitoring the beam flux was not operational at the time these samples were grown.
 - ¹⁹A. Ksendzov, W. T. Pike, and A. Larsson, *Phys. Rev. B* **47**, 2228 (1993).
 - ²⁰G. Bastard, *Wave Mechanics Applied to Semiconductor Heterostructures* (Halsted, New York, 1988).
 - ²¹G. Bastard, U. O. Ziemelis, C. Delalande, M. Voos, A. C. Gosard, and W. Wiegmann, *Solid State Commun.* **49**, 671 (1984); G. Duggan, *Proc. SPIE* **1283**, 206 (1990).
 - ²²M. Galluppi, L. Geelhaar, and H. Riechert, *Appl. Phys. Lett.* **86**, 131925 (2005).
 - ²³S. Datta, B. M. Arora, and S. Kumar, *Phys. Rev. B* **62**, 13604 (2000).
 - ²⁴P. R. C. Kent and A. Zunger, *Phys. Rev. Lett.* **86**, 2613 (2001).
 - ²⁵C. Skierbiszewski, P. Perlin, P. Wisniewski, W. Knap, T. Suski, W. Walukiewicz, W. Shan, K. M. Yu, J. W. Ager III, E. E. Haller, J. F. Geisz, and J. M. Olson, *Appl. Phys. Lett.* **76**, 2409 (2000).
 - ²⁶I. Vurgaftman and J. R. Meyer, *J. Appl. Phys.* **94**, 3675 (2003).
 - ²⁷Z. Pan, L. H. Li, Y. W. Lin, B. Q. Sun, D. S. Jiang, and W. K. Ge, *Appl. Phys. Lett.* **78**, 2217 (2001).
 - ²⁸M. Hetterich, M. D. Dawson, A. Yu. Egorov, D. Bernklau, and H. Riechert, *Appl. Phys. Lett.* **76**, 1030 (2000).
 - ²⁹R. J. Potter, N. Balkan, X. Marie, H. Carrère, E. Bedel, and G. Lacoste, *Phys. Status Solidi A* **187**, 663 (2001).
 - ³⁰P. J. Klar, H. Gruning, J. Koch, S. Schafer, K. Volz, W. Stolz, W. Heimbrod, A. M. Kamal Saadi, A. Lindsay, and E. P. O'Reilly, *Phys. Rev. B* **64**, 121203(R) (2001).
 - ³¹M. Hetterich, A. Grau, A. Yu. Egorov, and H. Riechert, *J. Appl. Phys.* **94**, 1810 (2003).
 - ³²W. Shan, W. Walukiewicz, K. M. Yu, J. W. Ager III, E. E. Haller, J. F. Geisz, D. J. Friedman, J. M. Olson, R. S. Kurtz, H. P. Xin, and C. W. Tu, *Phys. Status Solidi B* **223**, 75 (2001).
 - ³³J. Wu, W. Shan, W. Walukiewicz, K. M. Yu, J. W. Ager III, E. E. Haller, H. P. Xin, and C. W. Tu, *Phys. Rev. B* **64**, 085320 (2001); P. N. Hai, W. M. Chen, I. A. Buyanova, H. P. Xin, and C. W. Tu, *Appl. Phys. Lett.* **77**, 1843 (2000).